

1 **Meteorological constraints on oceanic halocarbons above the Peruvian**  
2 **Upwelling**

3

4 **S. Fuhlbrügge<sup>1</sup>, B. Quack<sup>1</sup>, E. Atlas<sup>2</sup>, A. Fiehn<sup>1</sup>, H. Hepach<sup>1</sup>, K. Krüger<sup>3</sup>**

5 [1] GEOMAR Helmholtz Centre for Ocean Research Kiel, Kiel, Germany

6 [2] Rosenstiel School for Marine and Atmospheric Sciences, Miami, Florida, USA

7 [3] Department of Geosciences, University of Oslo, Oslo, Norway

8 Correspondence to: K. Krüger ([kirstin.krueger@geo.uio.no](mailto:kirstin.krueger@geo.uio.no))

## Relevant changes made to the manuscript

- Section “2.3 Atmospheric VSLs” and “2.4 Oceanic VSLs concentrations and sea – air flux” have been combined to Section “2.3 Atmospheric and oceanic VSLs measurements and sea-air fluxes” according to the reviewers suggestion.
- Section 2.5 is now Section 2.4
- Section 2.6 is now Section 2.5
- Minor changes according to the Co-Editor report.

Changes made to the manuscript are marked **blue (new)** and **red (deleted)**.

## ***Response to Editor and Reviewer 2***

We would like to thank the Editor and Reviewer 2 for their suggestions to further improve the manuscript. Below you find our answers to your specific points.

*Editor:*

*The introduction is focussing on upwelling regions, however, the relevance of halocarbon emissions from upwelling regions in a global context is not mentioned. Therefore, an additional sentence mentioning the global distributions of oceanic halocarbon sources/fluxes would be very helpful to illustrate the significance of upwelling regions in relation to other oceanic regions. See e.g. Quack & Wallace (2003) and Butler et al. (2007)*

Author response:

We agree with the Editor and added the following sentence to the introduction: “[...] processes in the productive waters of the upwelling. Although oceanic upwelling and nearshore regions are small compared to the global ocean area, they are known to significantly contribute to the oceanic bromocarbon fluxes (Quack and Wallace, 2003; Butler et al., 2007; Ziska et al., 2013). In the upwelling regions the [...]”.

*Reviewer:*

*Line 39 - I don't think "confirms" is a good word here. It implies some great controversy where there is none. "underscores" might be a better word.*

Author response:

We agree with the reviewer and exchanged “confirms” with “underscores”.

*Reviewer:*

*Lines 168-187 -- These two sections should be combined. Section 2.3 does not have enough substance to warrant it being a separate section.*

Author response:

We agree with the reviewer and combined both section to “2.3 Atmospheric and oceanic VSLs measurements and sea-air fluxes”.

*Reviewer:*

*Line 169 - although the authors changed "was" to "were", I believe "was" is correct, as the subject of the sentence ("total") is singular. (That might depend upon which English is being considered, however.)*

Author response:

Done.

*Reviewer:*

*Line 212 - "three to six hourly" is a little awkward. Perhaps "every three to six hours, coincident with VLSL measurements . . ."?*

Author response:

We agree and changed the sentence to "Trajectories were released every three to six hours coincident with VLSL measurements along the cruise track on R/V METEOR."

*Reviewer:*

*Line 509 - insert "near-surface" between "observed" and "atmospheric"*

Author response:

Done.

*Reviewer:*

*Line 577 - insert apostrophe in "ships"*

Author response:

Done.

*Reviewer:*

*Line 676 - Again, I think "confirms" is the wrong word. They might want to try " .... demonstrates the close linkage between VLSL abundance and stability of the MABL."*

Author response:

Done.

*Reviewer:*

*Line 708 (Figure 2) - Should the advective delivery have an arrow at the top of the box? It seems the "convective loss" as used here is really a net flux and therefore incorporates any top down flux. If that's so, then it would be illogical to re-assert that flux as advective delivery. (This does not affect their computations, but I believe would be more consistent with their interpretation of the paper.)*

Author response:

The stable atmospheric conditions in the region suppress the downward movement of air through the inversion layers. Therefore we included the top down flux as residual in the "advective loss" term, which is illustrated with the arrow at the top of the Advective Delivery box in Figure 2.

1 **Meteorological constraints on oceanic halocarbons above the Peruvian**  
2 **Upwelling**

3

4 **S. Fuhlbrügge<sup>1</sup>, B. Quack<sup>1</sup>, E. Atlas<sup>2</sup>, A. Fiehn<sup>1</sup>, H. Hepach<sup>1</sup>, K. Krüger<sup>3</sup>**

5 [1] GEOMAR Helmholtz Centre for Ocean Research Kiel, Kiel, Germany

6 [2] Rosenstiel School for Marine and Atmospheric Sciences, Miami, Florida, USA

7 [3] Department of Geosciences, University of Oslo, Oslo, Norway

8 Correspondence to: K. Krüger (kirstin.krueger@geo.uio.no)

9

10 **Abstract**

11 During a cruise of R/V METEOR in December 2012 the oceanic sources and emissions of  
12 various halogenated trace gases and their mixing ratios in the marine atmospheric boundary  
13 layer (MABL) were investigated above the Peruvian Upwelling. This study presents novel  
14 observations of the three very short lived substances (VSLS): bromoform, dibromomethane  
15 and methyl iodide, together with high resolution meteorological measurements, Lagrangian  
16 transport and source-loss calculations. Oceanic emissions of bromoform and dibromomethane  
17 were relatively low compared to other upwelling regions, while those for methyl iodide were  
18 very high. Radiosonde launches during the cruise revealed a low, stable MABL and a distinct  
19 trade inversion above acting as strong barriers for convection and vertical transport of trace  
20 gases in this region. Observed atmospheric VSLS abundances, sea surface temperature,  
21 relative humidity and MABL height correlated well during the cruise. We used a simple  
22 source-loss estimate to quantify the contribution of oceanic emissions along the cruise track  
23 to the observed atmospheric concentrations. This analysis showed that averaged,  
24 instantaneous emissions could not support the observed atmospheric mixing ratios of VSLS  
25 and that the marine background abundances below the trade inversion were significantly  
26 influenced by advection of regional sources. Adding to this background, the observed  
27 maximum emissions of halocarbons in the coastal upwelling could explain the high  
28 atmospheric VSLS concentrations in combination with their accumulation under the distinct  
29 MABL and trade inversions. Stronger emissions along the near-shore coastline likely added

30 | to the elevated abundances under the steady atmospheric conditions. This study **confirms**  
31 | **underscores** the importance of oceanic upwelling and trade wind systems on the atmospheric  
32 | distribution of marine VSLs emissions.

### 33 | **1. Introduction**

34 | Oceanic fluxes of short-lived halocarbons contribute to reactive halogens in the atmosphere,  
35 | where they are subsequently involved in ozone chemistry, aerosol formation, and other  
36 | chemical cycles that influence the fate of pollutants and climate (McGivern et al., 2000; Saiz-  
37 | Lopez and von Glasow, 2012; Simpson et al., 2015). Recent studies have identified open  
38 | ocean upwelling areas in the Atlantic as large source regions for a number of brominated and  
39 | iodinated oceanic trace gases (Quack et al., 2004; Quack et al., 2007; O'Brien et al., 2009;  
40 | Raimund et al., 2011; Hepach et al., 2015b). Their sources are related to biological and  
41 | chemical processes in the productive waters of the upwelling. **Although oceanic upwelling**  
42 | **and nearshore regions are small compared to the global ocean area, they are known to**  
43 | **significantly contribute to the oceanic bromocarbon fluxes (Quack and Wallace, 2003; Butler**  
44 | **et al., 2007; Ziska et al., 2013). In the upwelling regions** the compounds are emitted from the  
45 | ocean and are horizontally transported and vertically mixed in the marine atmospheric  
46 | boundary layer (MABL) (Carpenter et al., 2010). Meteorological conditions strongly  
47 | influenced the atmospheric mixing ratio of the marine compounds bromoform (CHBr<sub>3</sub>),  
48 | dibromomethane (CH<sub>2</sub>Br<sub>2</sub>) and also methyl iodide (CH<sub>3</sub>I) (e.g. Fuhlbrügge et al., 2013;  
49 | Hepach et al., 2014). The combination of a pronounced low MABL above cold upwelling  
50 | waters with high concentrations and emissions of the compounds causes elevated  
51 | atmospheric mixing ratios. In a negative feedback process, these high atmospheric mixing  
52 | ratios reduce the marine emissions through a decrease of the sea-air concentration gradient  
53 | (Fuhlbrügge et al., 2013). Similar relationships would be expected for other oceanic  
54 | upwelling areas, where not only the oceanic emissions, but also meteorological conditions in  
55 | the lowermost atmosphere, i.e., the height, type and structure of the boundary layer and trade  
56 | inversion, determine the VSLs abundance and atmospheric distribution. The intense oceanic  
57 | upwelling in the Southeast Pacific off the coast of Peru transports large amounts of  
58 | subsurface water to the ocean surface and creates one of the most productive oceanic regions  
59 | worldwide (Codispoti et al., 1982). We therefore expect elevated levels of short-lived  
60 | halocarbons in the Peruvian Upwelling zone as potential source for the atmosphere. Indeed,  
61 | Schönhardt et al. (2008) detected elevated IO columns during September and November 2005

62 along the Peruvian coast with the SCIAMACHY satellite instrument and implied elevated  
63 iodine source gases from the Peruvian Upwelling.

64 Although recent studies investigated halocarbons in the East Pacific (Yokouchi et al., 2008;  
65 Mahajan et al., 2012; Saiz-Lopez et al., 2012; Gómez Martin et al., 2013; Liu et al., 2013),  
66 few have concentrated on the Peruvian Upwelling in the Southeast Pacific. Only  
67 measurements of methyl iodide exist in this region, revealing atmospheric abundances of 7  
68 ppt (Rasmussen et al., 1982). Observations of bromocarbons above the Peruvian Upwelling  
69 are currently lacking.

70 In this study we present a novel dataset of meteorological parameters, oceanic concentrations  
71 and atmospheric abundances of VSLs and calculated emissions along the Peruvian coast and  
72 in the Upwelling. The goal of this study is to assess the influence of oceanic upwelling and  
73 meteorological conditions on the atmospheric VSLs abundances above the Peruvian  
74 Upwelling, and to determine the contribution of the local oceanic emissions to MABL and  
75 free tropospheric VSLs concentrations.

76

## 77 **2. Data and Methods**

78 The cruise M91 on R/V METEOR from December 01 to 26, 2012 started and ended in Lima,  
79 Peru (Figure 1a). The ship reached the most northern position during the cruise on December  
80 03, 2012 at 5° S. In the following three weeks the ship headed southward and reached its  
81 southernmost position at 16° S on December 21, 2012. During this time the track alternated  
82 between open ocean sections and sections close to the Peruvian coast (up to 10 km distance)  
83 in the cold upwelling waters. A focus on diurnal variations was accomplished by 24-hour  
84 sampling at six stations along the cruise track.

85

### 86 **2.1 Meteorological observations**

87 Meteorological observations of surface air temperature (SAT), sea surface temperature (SST),  
88 relative humidity, air pressure, wind speed and direction were taken every second at about 25  
89 m height above sea level on R/V METEOR and averaged to 10 minute intervals for our  
90 investigations. Atmospheric profiles of temperature, wind, and humidity were obtained by 98  
91 radiosonde launches (0, 6, 12, 18 UTC) and additionally at three hour intervals during the  
92 diurnal stations along the cruise track, using Vaisala RS92 radiosondes. Due to permission  
93 limitations, radiosondes could not be launched within 12 nautical miles of the Peruvian coast.  
94 The collected radiosonde data was integrated in near real time into the Global  
95 Telecommunication System (GTS) to improve operational weather forecast models and



96 meteorological reanalysis for this region, which were used as input parameters for our  
97 trajectory calculations.

98

## 99 **2.2 MABL**

100 The radiosonde data are used to identify the height of the MABL, which is the atmospheric  
101 surface layer above the ocean in which trace gas emissions are mixed on a short time scale of  
102 an hour or less by convection and turbulence (Stull, 1988). Two different kinds of MABL can  
103 be distinguished that are characterized by the gradient of the virtual potential temperature  $\theta_v$ .  
104 A negative or neutral gradient reveals an *unstable convective layer*, while a positive gradient  
105 reveals a *stable* atmospheric layer. In case of an increase of the virtual potential temperature  
106 (positive gradient) near the surface, mixing in the MABL is suppressed. The upper limit of  
107 the convective MABL is set by a stable layer, e.g., a temperature inversion or a significant  
108 reduction in air moisture and is typically found above open ocean regions between 100 m and  
109 3 km height (Stull, 1988; Seibert et al., 2000). For determining the height of this stable layer  
110 above the convective MABL, we use the practical approach described in Seibert et al. (2000)  
111 and compute the virtual potential temperature for which an increase with altitude indicates  
112 the base of a stable layer. In this study, its base is increased by half of its thickness, which is  
113 the definition for the MABL height. Over oceanic upwelling regions the stable layer can even  
114 descend to the ocean surface (e.g. Höflich et al., 1972 and Fuhlbrügge et al., 2013).

115 Estimates for atmospheric surface stability and MABL conditions can be also obtained from  
116 variations of the surface humidity. While the absolute humidity determines the amount of  
117 water in a specific volume of air, the relative humidity is the ratio of the partial pressure of  
118 water vapour to the equilibrium vapour pressure at the observed temperature. Variations of  
119 the SAT directly influence the relative humidity at the surface (Section 3.1). Elevated relative  
120 humidity in this oceanic region likely points to stable layers with suppressed mixing of  
121 surface air and to a low and stable MABL height. Relative humidity is also used to derive the  
122 MABL height above the upwelling areas close to the coast, where radiosonde launches were  
123 not permitted (Section 2.1). We applied a multiple linear regression (Eq. 1), using  
124 meteorological parameters along the cruise track that had significant correlations (see Section  
125 3.5) with the observed MABL height (relative humidity ( $x_1$ ), SAT ( $x_2$ ), SST ( $x_3$ ) and wind  
126 speed ( $x_4$ )):

127

$$MABL\ height = b_1x_1 + b_2x_2 + b_3x_3 + b_4x_4 \quad (\text{Eq. 1})$$

with  $b_1 = -0.0117$ ;  $b_2 = 0.0202$ ;  $b_3 = 0.0467$ ;  $b_4 = 0.0089$

128

129 Missing MABL data close to the coast were then completed with the regressed MABL height  
130 (Eq. 1) at the VLSL sampling location.

131

### 132 **2.3 Atmospheric and oceanic VLSL measurements and sea-air fluxes**

133 A total of 198 air samples ~~were~~ ~~was~~ collected at three hourly intervals during the cruise at  
134 about 20 m height above sea level on the 5<sup>th</sup> superstructure deck of R/V METEOR using a  
135 portside jib of 5 – 6 m. The air samples were pressurized to 2 atm in pre-cleaned stainless  
136 steel canisters with a metal bellows pump and were analysed at the Rosenstiel School for  
137 Marine and Atmospheric Sciences (RSMAS, Miami, Florida) within six months after the  
138 cruise. Details about the analysis, the instrumental precision and the preparation of the  
139 samples are described in Schauffler et al. (1999) and Fuhlbrügge et al. (2013). The VLSL  
140 atmospheric mixing ratios were calculated with a NOAA standard (SX3573) from  
141 GEOMAR.

142

### 143 ~~2.4 Oceanic VLSL concentrations and sea – air flux~~

144 Starting after December 9, 2012, 102 water samples were taken at three hour intervals at a  
145 depth of 6.8 m from a continuously working water pump in the hydrographic shaft, an  
146 opening in the base of the ship hull of R/V Meteor. The samples were then analysed for  
147 bromoform, dibromomethane and methyl iodide and other halogenated trace gases by a purge  
148 and trap system attached to a gas chromatograph combined with an ECD (electron capture  
149 detector). The analysis has a precision of 10 % ( $1\sigma$ ) determined from duplicate samples. The  
150 approach is described in detail by Hepach et al. (2014).

151 The sea – air flux ( $F$ ) of bromoform, dibromomethane and methyl iodide is calculated with  $k_w$   
152 as transfer coefficient and  $\Delta c$  as concentration gradient between the water and equilibrium  
153 water concentration determined from the atmospheric concentrations (Eq. 2). The transfer  
154 coefficient was determined by the air – sea gas exchange parameterization of Nightingale et  
155 al. (2000) after a Schmidt number ( $Sc$ ) correction for the three gases (Eq. 3).

156

$$F = k_w \cdot \Delta c \quad (\text{Eq. 2})$$

157

$$k_w = k_{CO_2} \cdot \frac{Sc^{-\frac{1}{2}}}{600} \quad (\text{Eq. 3})$$

158

159 Details on deriving the air – sea concentration gradient and emissions are further described in  
160 Hepach et al. (2014) and references therein.

161

#### 162 | **2.52.4 Trajectory calculations**

163 The Lagrangian Particle Dispersion Model FLEXPART of the Norwegian Institute for Air  
164 Research in the Department of Atmospheric and Climate Research (Stohl et al., 2005) was  
165 used for trajectory calculations to analyse the air mass origins and the transport of surface air  
166 masses along the cruise track to the free troposphere (Stohl et al., 1998; Stohl and Trickl,  
167 1999). The model includes moist convection and turbulence parameterizations in the  
168 atmospheric boundary layer and free troposphere (Stohl and Thomson, 1999; Forster et al.,  
169 2007). We use the ECMWF (European Centre for Medium-Range Weather Forecasts)  
170 reanalysis product ERA-Interim (Dee et al., 2011) with a horizontal resolution of 1° x 1° and  
171 60 vertical model levels as meteorological input fields, providing air temperature, horizontal  
172 and vertical winds, boundary layer height, specific humidity, as well as convective and large  
173 scale precipitation with a six hourly temporal resolution. Trajectories were released every  
174 three to six ~~hourly hours at the time and position of the coincident~~ with VLSL measurements  
175 along the cruise track on R/V METEOR. At each of these release points 10,000 forward- and  
176 50 back-trajectories with a total runtime of ~30 days were initiated from the ocean surface  
177 within ± 30 minutes and ~20 m distance of the measurements. In total 98 release points for  
178 the forward- and back-trajectory calculations were analysed, determined by the spatial  
179 resolution of ERA-Interim data along the Peruvian coast, defining the land-sea mask of our  
180 trajectory calculations.

181

#### 182 | **2.62.5 Oceanic contribution to MABL VLSL abundances**

183 To estimate the contribution of local oceanic sources to the atmospheric mixing ratios in the  
184 lowermost atmosphere above the Peruvian Upwelling, we apply a mass balance concept to  
185 the oceanic emissions, the time scales of air mass transport and the chemical loss (Fuhlbrügge  
186 et al., 2016). First we define a box above each release event with a size of ~400 m<sup>2</sup> around  
187 the measurement location and the height of the MABL and assume steady-state in the box  
188 (Figure 2). During each trajectory release event we assume the specific sea-air flux to be  
189 constant and the emissions to be homogeneously mixed within the box. Then the contribution

190 of the sea-air flux is computed as the ratio of the VSLS flux from the ocean into the MABL  
 191 (in mol per day) and the total amount of VSLS in the box (in mol). This ratio is defined as the  
 192 Oceanic Delivery (OD) and is given in percentage per day. In addition to the delivery of  
 193 oceanic VSLS to the box, the loss of VSLS out of the box into the free troposphere is defined  
 194 as the Convective Loss (COL) and this quantity is derived from the mean residence time of  
 195 the FLEXPART trajectories in the box during each release event. Note that the COL indicates  
 196 the loss of surface air due to all kinds of vertical movement out of the box. Since this is a loss  
 197 process, COL is given as a negative quantity expressed as percentage per day. The chemical  
 198 degradation of VSLS by OH and photolysis in the MABL is calculated from the chemical  
 199 lifetime of each compound in the MABL. We use lifetimes of 15 days for bromoform, 94  
 200 days for dibromomethane and 4 days for methyl iodide (Carpenter et al., 2014) ,  
 201 representative for the tropical boundary layer. The Chemical Loss (CL) is given as a negative  
 202 quantity in percentage per day. OD, COL and CL must be balanced by an advective transport  
 203 of air masses in and out of the box. The change of the VSLS through advective transport is  
 204 defined as Advective Delivery (AD) and also is given in percentage per day.

205 To estimate the relative importance of ocean emissions (OD) to the halocarbon loss through  
 206 vertical mixing (COL) we define an Oceanic Delivery Ratio (ODR) (Eq. 4) as the ratio  
 207 between OD and COL:

$$208 \quad ODR = \frac{OD [\%d^{-1}]}{COL [\%d^{-1}]} = \frac{Sea-Air \text{ flux contribution } [\%d^{-1}]}{Loss \text{ of box air to the FT } [\%d^{-1}]} \quad (\text{Eq. 4})$$

209

210 Similarly, the Chemical Loss in the box (CL) and the change in VSLS due to advection (AD)  
 211 are related to COL to get the Chemical Loss Ratio (CLR) and the Advective Delivery Ratio  
 212 (ADR). From mass balance considerations,  $ODR - CLR + ADR = 1$ . Since CL, OD and AD  
 213 are divided by COL, ratios for source processes are positive and negative for loss processes  
 214 (Fuhlbrügge et al., 2016).

215

### 216 **3. Observations on R/V METEOR**

#### 217 **3.1. Meteorology**

218 The Peruvian coast is dominated by the southern hemisphere trade wind regime with  
 219 predominantly south-easterly winds (Figure 1). The Andes, which are known to act as a  
 220 barrier to zonal wind in this region, affect the horizontal air mass transport along the coast  
 221 (Figure 1b-d). The steeply sloping mountains at the coast form strong winds parallel to the

222 South American coastline (Garreaud and Munoz, 2005). The 10-day back-trajectories reveal  
223 a mix of open ocean and coastal air-masses (Figure 1). The average wind direction observed  
224 on R/V Meteor during the cruise is  $160^\circ \pm 34^\circ$  (mean  $\pm \sigma$ ) with a moderate average wind  
225 speed of  $6.2 \pm 2.2 \text{ ms}^{-1}$  (Figure 3b). ERA-Interim reveals similar winds along the cruise track  
226 with a mean wind speed of  $5.6 \pm 1.8 \text{ ms}^{-1}$  and a mean wind direction of  $168^\circ \pm 21^\circ$  (not  
227 shown here). The divergence of the wind driven Ekman transport along the Peruvian coast  
228 leads to the observed oceanic upwelling of cold waters. The most intense upwelling was  
229 observed several times near the coast where both SST and SAT rapidly drop from  $19 - 22^\circ\text{C}$   
230 to less than  $18^\circ\text{C}$  (Figure 3a). The impact of the cold upwelling water on the air masses is  
231 also visible in the observed humidity fields (Figure 3c). Here, the decreasing SAT reduces the  
232 amount of water vapour that the surface air is able to contain, leading to an increase of the  
233 relative humidity and indicating a stable atmospheric surface layer with suppressed vertical  
234 mixing. The absolute humidity stays constant or even decreases above the oceanic upwelling  
235 due to condensation of water vapour when surface air cools and becomes saturated,  
236 coinciding with fog observations on the ship. A decrease of the absolute humidity outside the  
237 upwelling points to a change in advected air masses (e.g. Dec 9, 11, 19, 2012; Figure 3c).

238

### 239 **3.2. VLSL abundances and oceanic emissions**

240 Surface water samples of the coastal upwelling areas show elevated VLSL concentrations  
241 compared to the open ocean for all compounds, especially for methyl iodide (Hepach et al.,  
242 2016, in review). Atmospheric mixing ratios of bromoform were on average  $2.91 \pm 0.68$  ppt  
243 (Table 1). Dibromomethane mixing ratios (average  $1.25 \pm 0.26$  ppt) show a similar pattern  
244 and good correlation with bromoform (Table 3). Elevated mixing ratios for all three  
245 compounds are generally found above the intense cold oceanic upwelling regions close to the  
246 Peruvian coast (Figure 3e). While the bromocarbons double above the upwelling, methyl  
247 iodide mixing ratios increase up to 5-fold, demonstrating its stronger accumulation in the low  
248 and stable boundary layer.

249 The concentration ratio of atmospheric dibromomethane to bromoform can be used as an  
250 indicator of bromocarbon sources along coastal areas. Low ratios of about 0.1 have been  
251 observed in coastal source regions and have been interpreted as the emission ratios of macro  
252 algae (Yokouchi et al., 2005; Carpenter et al., 2003). The shorter chemical lifetime of  
253 bromoform (15 days) in contrast to dibromomethane (94 days) in the boundary layer leads to  
254 an increase of the ratio during transport as long as the air mass is not newly enriched with  
255 bromoform (Carpenter et al., 2014). This concentration ratio generally decreased from the

256 North to the South (Figure 3f), implying an intensification of fresh bromoform sources  
257 towards the southern part of the cruise track, which is also reflected by increasing water  
258 concentrations. Atmospheric methyl iodide measurements along the cruise track reveal a  
259 mean mixing ratio of  $1.54 \pm 0.49$  ppt, which, similar to the two bromocarbons, maximizes  
260 over the coastal upwelling regions (Figure 3e).

261 Oceanic emissions during the cruise were calculated from the approximately synchronous  
262 measurements of sea water concentrations and atmospheric mixing ratios, sea surface  
263 temperatures and wind speeds, measured on R/V METEOR. Oceanic concentrations and  
264 atmospheric mixing ratios of each compound were weakly or not at all correlated ( $R_{\text{bromoform}} =$   
265  $0.00$ ,  $R_{\text{dibromomethane}} = 0.29$  and  $R_{\text{methyl iodide}} = 0.34$ ). Mean sea-air fluxes of the bromocarbons  
266 during the cruise are low with  $117 \pm 492$  pmol m<sup>-2</sup> h<sup>-1</sup> for bromoform and  $245 \pm 299$  pmol m<sup>-2</sup>  
267 h<sup>-1</sup> for dibromomethane compared to other oceanic regions (e.g. Fuhlbrügge et al., 2013;  
268 Hepach et al., 2015a), but for methyl iodide the fluxes were elevated with  $856 \pm 623$  pmol m<sup>-2</sup>  
269 h<sup>-1</sup> (Figure 3g, Table 1). Further investigations of the distributions and sources of iodinated  
270 compounds during this cruise are carried out by Hepach et al. (2016, in review).

271

### 272 **3.3. Lower atmosphere conditions**

273 A strong positive vertical gradient of relative humidity at ~1 km height (Figure 4a) indicates  
274 an increase of the atmospheric stability. This convective barrier, known as the trade inversion  
275 (Riehl, 1954, 1979; Höflich, 1972), is also reflected in the meridional wind (Figure 4b).  
276 Below ~1 km altitude the south-easterly trade winds create a strong positive meridional wind  
277 component, also visible in the forward trajectories (Figure 1c-d). The flow of air masses in  
278 the Hadley Cell back to the subtropics causes a predominantly northerly wind above ~1 km  
279 height. The intense increase of  $\theta_v$  in combination with the relative humidity decrease and the  
280 wind shear at ~1 km height identifies this level as a strong vertical transport barrier (Figure  
281 4c). Above the cold upwelling water, temperature inversions create additional stable layers  
282 above the surface, leading to very low MABL heights of < 100 m, e.g., on December 03, 08  
283 or 17, 2012 and to a reduced vertical transport of surface air. The mean MABL height from  
284 the radiosonde observations is  $370 \pm 170$  m (ERA-Interim  $376 \pm 169$  m). The relative  
285 humidity, SAT, SST and wind speed show significant correlations with the observed MABL  
286 height (Table 3). The regressed MABL heights (Section 2.2) show a distinct decrease above  
287 the cold upwelling regions close to the coast with  $158 \pm 79$  m on average. Taking the  
288 regressed MABL height into account, the mean MABL height during the cruise decreases to  
289  $307 \pm 177$  m. The stable atmospheric conditions from the surface to the trade inversion lead

290 to strong transport barriers also visible in the accumulation of below 2-day old air masses  
291 within the first kilometre of the atmosphere (Figure 4d).

292

### 293 **3.4. Contribution of oceanic emissions to VSLS abundances in the MABL**

294 We estimate the contribution of oceanic emissions to mixing ratios within the MABL and  
295 below the trade inversion with a VSLS source-loss estimate (Table 2). The mean loss of  
296 VSLS out of the MABL box is  $351.0 \text{ \% d}^{-1}$  and equal for all compounds, since it is computed  
297 from the loss of trajectories out of the box. The loss is based on a mean residence time of the  
298 FLEXPART trajectories of 7 hours in the observed in-situ MABL height during the cruise.  
299 The ratio of the individual OD of each compound and the COL at this location results in the  
300 particular ODR for each compound. The ODR reveals that on average only 3 % of the  
301 observed atmospheric bromoform in the MABL originates from local oceanic emissions and  
302 99 % are advected including a chemical loss of 2 %. The numbers show that the observed  
303 mean atmospheric concentrations cannot be explained by the mean local oceanic emissions.  
304 While the surface air masses can leave the MABL within hours, they are suppressed from  
305 entering the free troposphere through the trade inversion. FLEXPART trajectories indicate an  
306 average residence time of air 48 h below the average trade inversion height of 1.1 km. During  
307 the 48 h and the prevailing southerly mean wind speed of 6.2 m/s oceanic VSLS emissions  
308 can accumulate over a fetch of  $10^\circ$  latitude. The impact of these conditions on VSLS  
309 emissions is discussed in Section 4.

310

### 311 **3.5. Meteorological constraints on atmospheric VSLS in the MABL**

312 We find significant high correlations between meteorological parameters and the abundances  
313 of bromoform, dibromomethane and methyl iodide (Table 3) along the Peruvian coast. The  
314 predominantly moderate winds during the cruise are negatively correlated with the  
315 atmospheric VSLS and positively correlated with the MABL height. This shows that VSLS  
316 abundances tend to be elevated during periods of lower wind speeds which lead to reduced  
317 mixing of surface air and therefore to lower MABL heights, in particular above the coastal  
318 upwelling events on December 11, 15-17 and 24, 2012. No significant correlation is found  
319 between the oceanic emissions and the atmospheric VSLS (not shown) revealing a stronger  
320 influence of the wind speed on the atmospheric accumulation of the VSLS rather than the  
321 oceanic emissions. SAT and SST both are negatively correlated with atmospheric VSLS,  
322 since elevated atmospheric VSLS mixing ratios are generally found close to the oceanic

323 upwelling regions with low SATs and SSTs. In these regions the decrease of the SATs leads  
324 to an increase of the relative humidity (Section 3.1), which results in a significantly high  
325 correlation with the VSLs. Since SAT and SST impact the MABL, which affects the relative  
326 humidity, these correlation coefficients are co-correlated. Correlation coefficients between  
327 the MABL height and the VSLs are slightly lower (Table 3). A principal component analysis  
328 of the parameters in Table 3 also confirmed the strong connection between SAT, SST,  
329 MABL height, relative humidity and atmospheric mixing ratios of bromoform and  
330 dibromomethane (not shown here).

331

### 332 **3.6. Comparison to other oceanic regions**

333 Surface water concentrations of bromoform in the Peruvian Upwelling during the cruise were  
334 generally lower compared to observations in other coastal upwelling regions, e.g., the  
335 Mauritanian Upwelling (Carpenter et al., 2010; Fuhlbrügge et al., 2013; Hepach et al., 2014).  
336 While dibromomethane concentrations are comparable, methyl iodide concentrations are  
337 almost eight times higher than in the Mauritanian Upwelling (Figure 3d, Table 1, Hepach et  
338 al., 2014). Atmospheric mixing ratios of bromoform and dibromomethane are significantly  
339 lower above the Peruvian Upwelling compared to observations above the Mauritanian  
340 Upwelling, while methyl iodide mixing ratios are comparable (Fuhlbrügge et al., 2013).

341 MABL properties (height and stability) reveal a stronger influence on the VSLs abundances  
342 at the marine surface during the DRIVE cruise covering the Mauritanian Upwelling  
343 compared to this study (M91) covering the Peruvian Upwelling (Figure 5). Observed local  
344 oceanic bromocarbon emissions can only partly explain the atmospheric VSLs  
345 concentrations above the Peruvian Upwelling, while above the Mauritanian Upwelling, the  
346 generally higher emissions could occasionally explain up to 100% of the atmospheric  
347 abundances of VSLs in very low and stable MABL conditions (Fuhlbrügge et al., 2013;  
348 Hepach et al., 2014). The predominantly southerly winds along the western coast line of Peru  
349 allowed only minor continental influence on the offshore coastal atmosphere, while the  
350 Mauritanian Upwelling showed a larger variation of maritime and continental air masses.  
351 Although our investigations revealed low MABL heights close to the Peruvian coast, the  
352 maritime air mass origin led to less developed surface inversions compared to those observed  
353 above the Mauritanian Upwelling, where the higher emissions led to a stronger and more  
354 variable enrichment in the MABL. This can lead to the observed higher correlation  
355 coefficients between the MABL height and the VSLs abundances in the Mauritanian  
356 Upwelling (Figure 5).



357 Compared to the two eastern boundary upwelling systems, observed VSLS sources at the  
358 coasts of the South China and Sulu seas were significantly higher (Fuhlbrügge et al., 2016).  
359 Despite the elevated emissions there, the atmospheric VSLS abundances in the West Pacific  
360 were lower, due to the presence of a convective active, well ventilated MABL. The  
361 comparison between the different regions demonstrates that the atmospheric abundances of  
362 VSLS over the ocean are significantly controlled by prevailing meteorological conditions  
363 next to their oceanic sources and emissions.

364

#### 365 **4. Discussion**

366 Compounds emitted from the Peruvian Upwelling are first homogeneously distributed within  
367 the MABL in only a few hours according to the observations during the M91 cruise.  
368 Afterwards the emitted compounds are distributed within and transported below the trade  
369 inversion. For air masses above or close to oceanic upwelling regions, the MABL height is  
370 the first transport barrier on short time scales, while the trade inversion acts as the second  
371 more pronounced barrier for vertical transport on longer time scales. The residence time of  
372 air masses below the trade inversion of 48 h leads to a stronger enrichment of VSLS from the  
373 oceanic emissions, reflected in the OD (Table 2), compared to the enrichment in the MABL.  
374 For the mean wind speed of  $6.2 \text{ ms}^{-1}$  and wind direction of  $160^\circ$  observed during the cruise,  
375 air masses accumulate oceanic emissions from approx.  $1.5^\circ$  latitude distance during the  
376 residence time of 7 hours in the MABL and below the trade wind inversion from approx.  $10^\circ$   
377 latitude during 48 hours, which covers the southern Peruvian as well as part of the Chilean  
378 coast.

379

#### 380 *Accumulation of background concentrations*

381 | The observed [near-surface](#) atmospheric mixing ratios suggest background concentrations of  
382 the compounds which were around 2 ppt for  $\text{CHBr}_3$ , 0.8 ppt of  $\text{CH}_2\text{Br}_2$  and 1 ppt for  $\text{CH}_3\text{I}$   
383 (Figure 3e and 5). The back-trajectories revealed air masses originating from the southern  
384 Peruvian and Chilean coast, which were transported along the coast for about 5 days. In  
385 combination with a stable MABL and a distinct trade inversion acting as strong barriers to the  
386 vertical mixing of trace gases, these air-masses travelled close to the surface where they  
387 could be enriched during 48 hours with regional emissions before they enter the free  
388 troposphere. Mean emissions of around  $2000 \text{ pmol m}^{-2} \text{ h}^{-1}$  for  $\text{CHBr}_3$  and for  $\text{CH}_3\text{I}$  and  $800$   
389  $\text{pmol m}^{-2} \text{ h}^{-1}$  for  $\text{CH}_2\text{Br}_2$  would have been needed during the residence time of 48 h of air  
390 below the trade wind inversion to reach the elevated background concentrations observed on-

391 board the ship. These emissions are close to the maximum observed during the cruise and are  
392 frequently observed in other coastal oceanic regions (Quack et al., 2003, Carpenter et al.,  
393 2000, 2015, Ziska et al., 2013). Thus, although our measurements along the cruise track did  
394 not reflect conditions that produced an average ocean emission rate sufficient to support high  
395 background VSLS abundances, we propose that higher emissions may be present at other  
396 times and locations along the coast, which were passed by the air mass trajectories (Figure 1)  
397 and added additional VSLS to the MABL. We suspect that waters very close to the coast,  
398 where generally elevated concentrations of the bromocarbons are found (Carpenter et al.,  
399 2005; Leedham et al., 2013; Ziska et al., 2013), might even be stronger source regions  
400 although these areas were not crossed by the cruise track.

401

#### 402 *Maximum mixing ratios in the coastal upwelling*

403 In addition to the background concentrations, Figure 5 shows the good correlation of MABL  
404 height and the three atmospheric VSLS. The slopes reveal approximately 0.5 ppt per 100 m  
405 MABL height for  $\text{CHBr}_3$ , 0.2 ppt for  $\text{CH}_2\text{Br}_2$  and 0.3 ppt for  $\text{CH}_3\text{I}$ , yielding mean maximum  
406 mixing ratios of around 4.5 ppt  $\text{CHBr}_3$ , 1.8 ppt for  $\text{CH}_2\text{Br}_2$  and 2.4 ppt for  $\text{CH}_3\text{I}$  in the lowest  
407 observed MABL heights. The difference of 2.5 ppt  $\text{CHBr}_3$ , 1.0 ppt for  $\text{CH}_2\text{Br}_2$  and 1.4 ppt for  
408  $\text{CH}_3\text{I}$  to the accumulated background concentration requires mean source fluxes of 2500  $\text{pmol}$   
409  $\text{m}^{-2} \text{h}^{-1}$  for  $\text{CHBr}_3$ , 1000 for  $\text{CH}_2\text{Br}_2$  and 1400 for  $\text{CH}_3\text{I}$  into a stable MABL height of 100 m  
410 during 4 h accumulation. Although the mean fluxes during the cruise were lower, higher  
411 fluxes of 2000  $\text{pmol m}^{-2} \text{h}^{-1}$   $\text{CHBr}_3$ , 1000 for  $\text{CH}_2\text{Br}_2$  and 4000 for  $\text{CH}_3\text{I}$  were occasionally  
412 observed especially near the coast line (Figure 3, Table 1), which plays an important role as  
413 source region for the trace gases. As an example, the same coastal upwelling region was  
414 crossed two times during the cruise (17 Dec and 25 Dec, 2012). While other conditions were  
415 similar, the wind direction on the second occasion was from the coast and the air showed  
416 elevated atmospheric mixing ratios compared to the first occasion. Thus, we strongly believe  
417 that major source regions for the accumulation of the VSLS below the stable MABL and the  
418 distinct trade wind inversion above the coastal upwelling are associated with the coastal  
419 upwelling waters and regions even closer to the coast lines, which are also under the  
420 influence of steady and stable meteorological conditions due to topography and the upwelling  
421 of cold waters along the Peruvian and Chilean coast. Overall, we suggest that the observed  
422 high atmospheric mixing ratios above the Peruvian Upwelling resulted from the close  
423 interaction between steady meteorological conditions, advection of elevated background air,  
424 increased atmospheric stability above the cold oceanic upwelling region, and VSLS sources

425 in the coastal upwelling itself and even closer to the shore line, which we were not able to  
426 examine during our cruise.

427

#### 428 *Transport from the upwelling*

429 After the air masses were observed on R/V METEOR, the 10 day forward trajectories  
430 revealed a near-surface transport towards the equator (Figure 1). These trajectories  
431 predominantly stayed below 1 km altitude due to the horizontal extent of the trade inversion.  
432 A contribution of oceanic emissions from the Peruvian Upwelling to the free troposphere is  
433 only achieved in the inner tropics after a transport time of 5 – 8 days, where the VLSL  
434 abundances were transported into higher altitudes. Since the lifetime of methyl iodide is only  
435 four days in the MABL a significant contribution of methyl iodide from the Peruvian  
436 Upwelling to observations made by Yokouchi et al. (2008) at San Cristobal, Galapagos can  
437 not be expected. However, it can partly explain the elevated IO observed above the Peruvian  
438 Upwelling (Schönhardt et al., 2008), which is further investigated by the companion study of  
439 Hepach et al. (2016, in review). The low contribution of oceanic emissions and boundary  
440 layer air to the free troposphere in this region is representative for the prevalent neutral El  
441 Niño Southern Oscillation (ENSO) conditions as were observed during December 2012  
442 (ENSO Diagnostic Discussion, NCEP/CPC issue, November 2012). Different ENSO  
443 conditions can be expected to influence VLSL air-sea interactions above the Peruvian  
444 Upwelling and should be investigated in future studies.

445

#### 446 *Uncertainties*

447 Uncertainties of our study may result from the applied method, which takes in-situ  
448 observations during the cruise and close to the ship's position into account. Although the  
449 cruise track covered a significant large area of the Peruvian Upwelling between 5° S and 16°  
450 S, elevated sea surface concentrations and emissions, especially closer to coast lines may  
451 have contributed to the observed VLSL abundances, which were not sampled during the  
452 cruise. In regions with low MABL heights very close to the coast, where the source-loss  
453 estimate could not be applied due to trajectory analysis gaps (Section- 2.4.2.5), potentially  
454 high emissions in combination with the stable atmospheric stratification could significantly  
455 increase the oceanic contribution to the MABL. Different parameterizations for the wind-  
456 based transfer coefficient  $k_w$ , as discussed in Lennartz et al. (2015) and Fuhlbrügge et al.  
457 (2016), lead only to an overall difference of 34% in the calculated oceanic emissions during  
458 M91, due to the relatively low prevailing winds. Additional uncertainties in our source-loss

459 estimate may arise from deficiencies in the meteorological input fields from ERA-Interim  
460 reanalysis as well as from the air mass transport simulated by FLEXPART, but these  
461 uncertainties are difficult to quantify. Both could lead to either a shorter or longer residence  
462 time of the surface air masses within the MABL or below the trade inversion. However,  
463 Fuhlbrügge et al. (2016) showed that differences in the MABL height of ERA-Interim and  
464 radiosonde observations affect the computed ODR only marginal. Further uncertainties may  
465 arise from spatial variations of the VSLs lifetimes and thus the chemical degradation of the  
466 compounds we used in this study. These effects are expected to be small for bromoform and  
467 dibromomethane since the overall impact of photochemical loss rates is only a few % of the  
468 total budget. The uncertainty in chemical loss rates for methyl iodide is larger, and more  
469 detailed photolysis rate calculations and actinic flux measurements would be useful to better  
470 constrain this process for compounds, whose main loss is through photolysis. Finally, future  
471 studies need to investigate in particular the near coastal processes and sources to estimate  
472 their contribution to the air-sea gas exchange and lower atmospheric VSLs abundances above  
473 the Peruvian Upwelling.

474

475

## 476 **5. Summary**

477 This study investigated the contribution of oceanic emissions to VSLs abundances in the  
478 lowermost atmosphere above coastal upwelling and open ocean regions along the Peruvian  
479 coast during December 2012. Meteorological data were obtained on R/V METEOR and by  
480 radiosondes up to the stratosphere. Oceanic VSLs emissions along the cruise track were  
481 determined from air and surface water measurements. The transport of air masses was  
482 calculated with FLEXPART trajectories using ERA-I reanalysis. All data was synthesized in  
483 a source-loss model, investigating the influences of VSLs emissions and atmospheric  
484 transport on the observed VSLs abundances.

485 Oceanic upwelling was observed close to the Peruvian coast, which strongly impacted  
486 meteorological conditions in this region. On average a low, stable MABL height of  $307 \pm 177$   
487 m was encountered during the cruise, decreasing to about 100 m above the upwelling. A  
488 distinct trade inversion at  $1.1 \pm 0.3$  km height was identified as the dominant transport barrier  
489 for MABL air into the free troposphere during the cruise. The halogenated VSLs bromoform  
490 and dibromomethane showed low average oceanic emissions of  $117 \pm 492$  pmol m<sup>-2</sup> h<sup>-1</sup> for  
491 bromoform and  $245 \pm 299$  pmol m<sup>-2</sup> h<sup>-1</sup> for dibromomethane, while methyl iodide emissions  
492 were elevated with  $856 \pm 623$  pmol m<sup>-2</sup> h<sup>-1</sup>. In contrast, the atmospheric mixing ratios of the

493 compounds were elevated compared to average open ocean regions with  $2.9 \pm 0.7$  ppt  
494 (bromoform),  $1.3 \pm 0.3$  ppt (dibromomethane) and  $1.5 \pm 0.5$  ppt (methyl iodide). The mean  
495 oceanic emissions along the cruise track explained on average 3 % (-8 to 33 %) of  
496 bromoform, 10 % (-5 to 45 %) of dibromomethane, and 28 % (3 to 80 %) of methyl iodide  
497 abundances in the MABL. Thus, the significant contribution of local oceanic VSLs emissions  
498 to the overlying atmosphere that we expected was not captured during the time and location  
499 of our sample collection, and showed the need for a separation of transported and local  
500 signals. The elevated atmospheric VSLs background concentrations in the region appear  
501 largely advected and enriched below the trade wind inversion during two days of transport  
502 from further south. The pronounced stable and steady atmospheric conditions close to the  
503 Peruvian and Chilean coast led during a few hours to an additional accumulation and increase  
504 of the atmospheric VSLs mixing ratios above the coastal upwelling, where stronger source  
505 regions are likely to exist close to the coast line, which have not been sampled during the  
506 cruise.

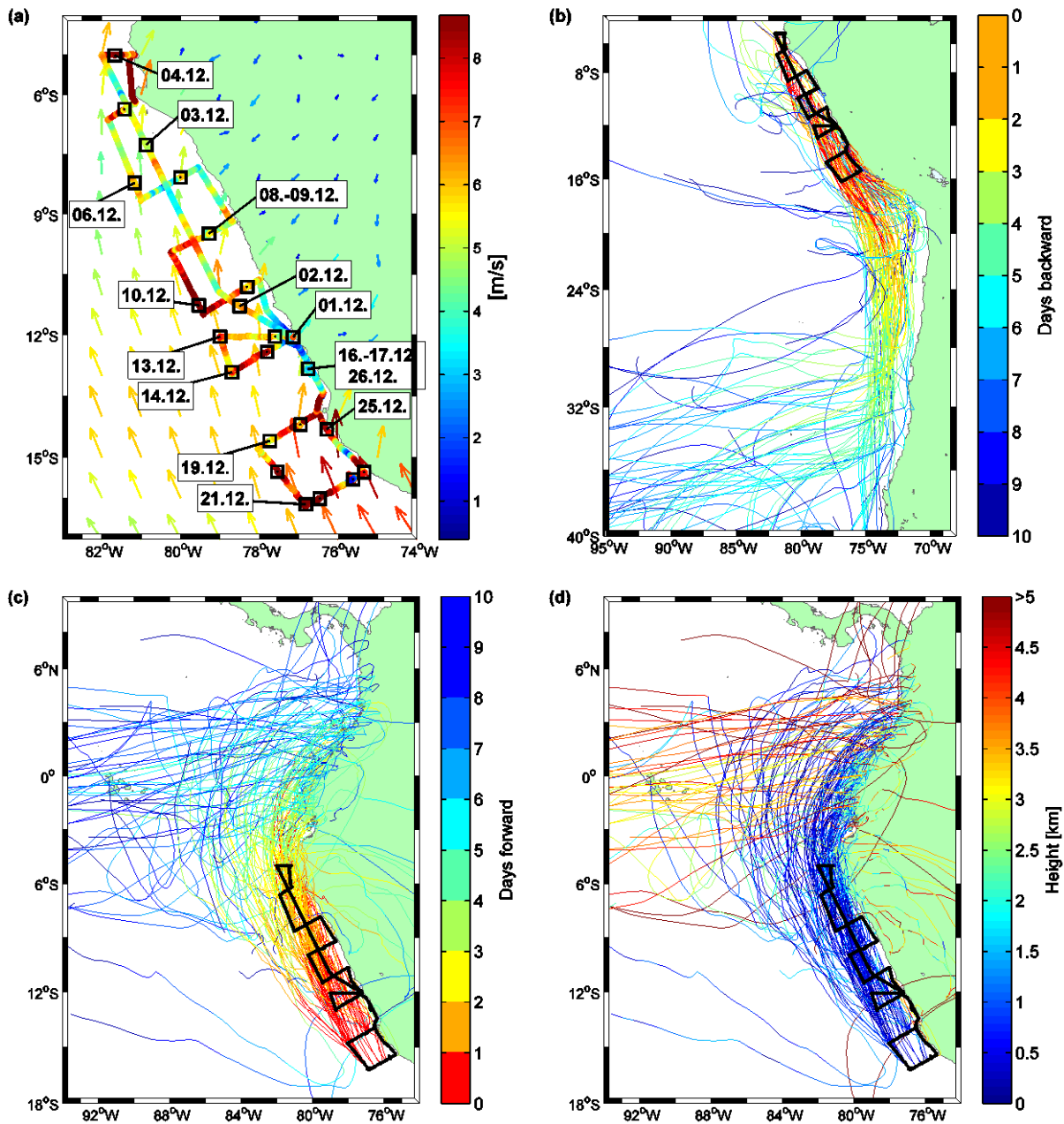
507 | Our study ~~confirms-demonstrates that elevated atmospheric~~the close linkage between VSLs  
508 abundances ~~above-oceanic-coastal-upwelling-regions-are-generally-related-with~~and stable  
509 stability ~~and-low~~of the MABLs. Additionally, a pronounced trade inversion can lead to a  
510 near-surface accumulation of the VSLs and thus also impacts oceanic emissions. Further  
511 studies are necessary to investigate the coastal and near shore source regions of the elevated  
512 atmospheric VSLs in the Peruvian Upwelling during different seasons and ENSO conditions.

513

514        **Acknowledgements**

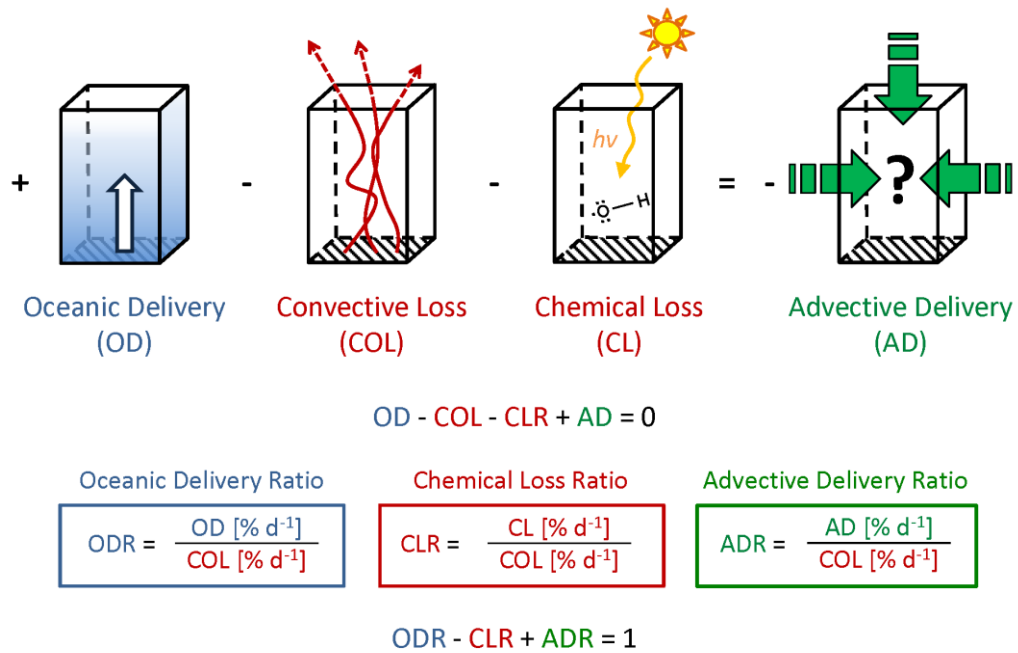
515        This study was supported by the BMBF grant SOPRAN II FKZ 03F0611A. We acknowledge  
516        the authorities of Peru for the permissions to work in their territorial waters. We thank the  
517        European Centre for medium range weather forecast (ECMWF) for the provision of ERA-  
518        Interim reanalysis data and the Lagrangian particle dispersion model FLEXPART used in this  
519        publication. We also like to thank the captain and crew of R/V METEOR, and the Deutscher  
520        Wetterdienst (DWD) for the support. EA acknowledges financial support of his work from  
521        the Upper Atmosphere Research Program of the US NASA.

522



524

525 Figure 1a-d: (a) 10 minute mean of wind speed observed on R/V METEOR displayed along  
 526 the cruise track; monthly mean (December 2012) of 10 m wind speed and direction from  
 527 ERA-Interim displayed as arrows. (b) Extract from 10-day FLEXPART back-trajectories  
 528 coloured according to the time until they reach the specific ship position on the cruise track of  
 529 R/V METEOR (black). (c) Extract from 10-day FLEXPART forward trajectories coloured  
 530 according to the time since they were released. (d) same as c) coloured according to the  
 531 height (km) of the trajectories.

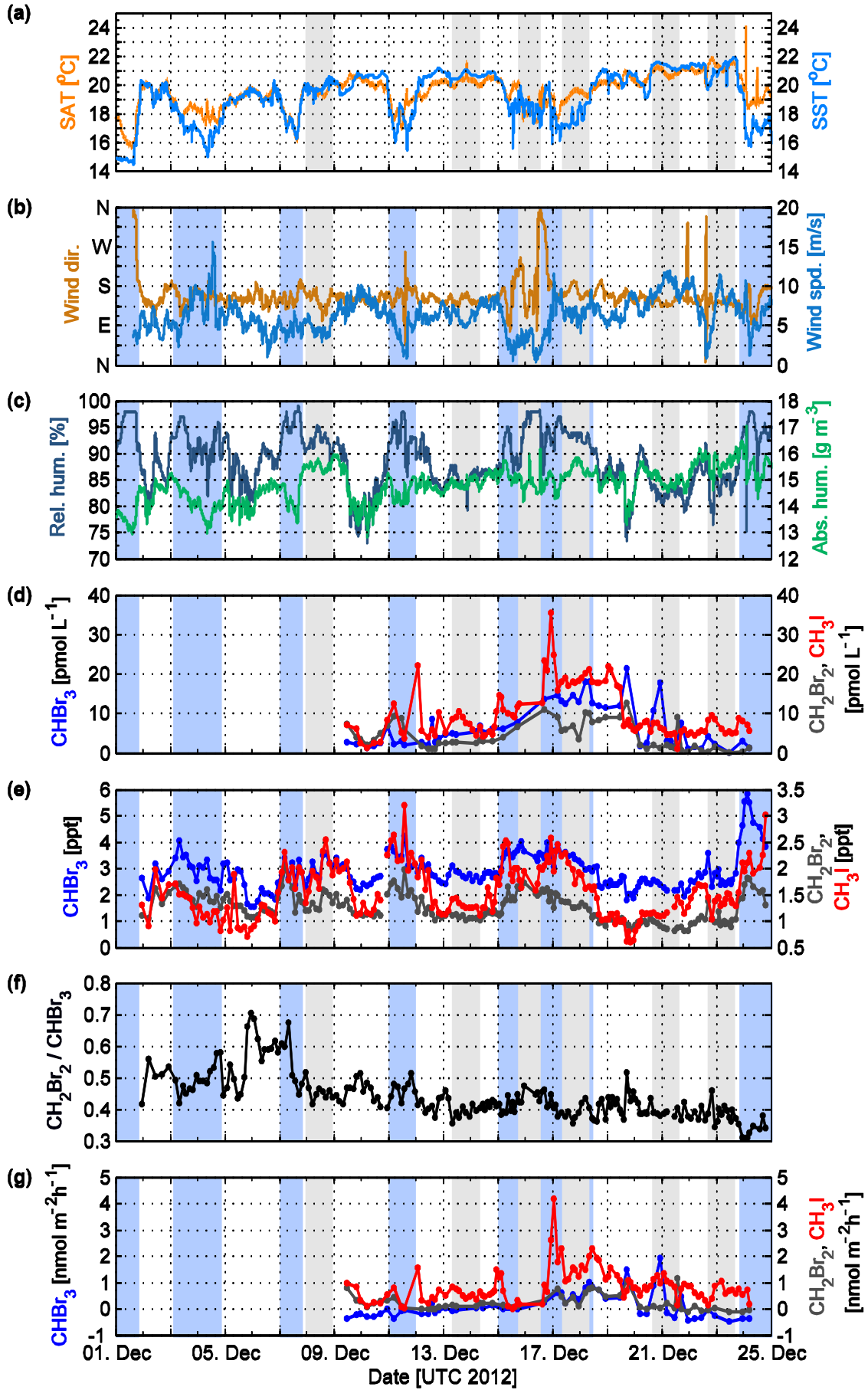


533

534 Figure 2: Schematic summary of the components of the applied mass-balance concept from  
 535 Fuhlbrügge et al. (2016): Oceanic Delivery (OD), the Convective Loss (COL), the Chemical  
 536 Loss (CL), the Advective Delivery (AD), the Oceanic Delivery Ratio (ODR), the Chemical  
 537 Loss Ratio (CLR) and the Advective Delivery Ratio (ADR). The shaded area reflects an area  
 538 of 400 m<sup>2</sup>.

539



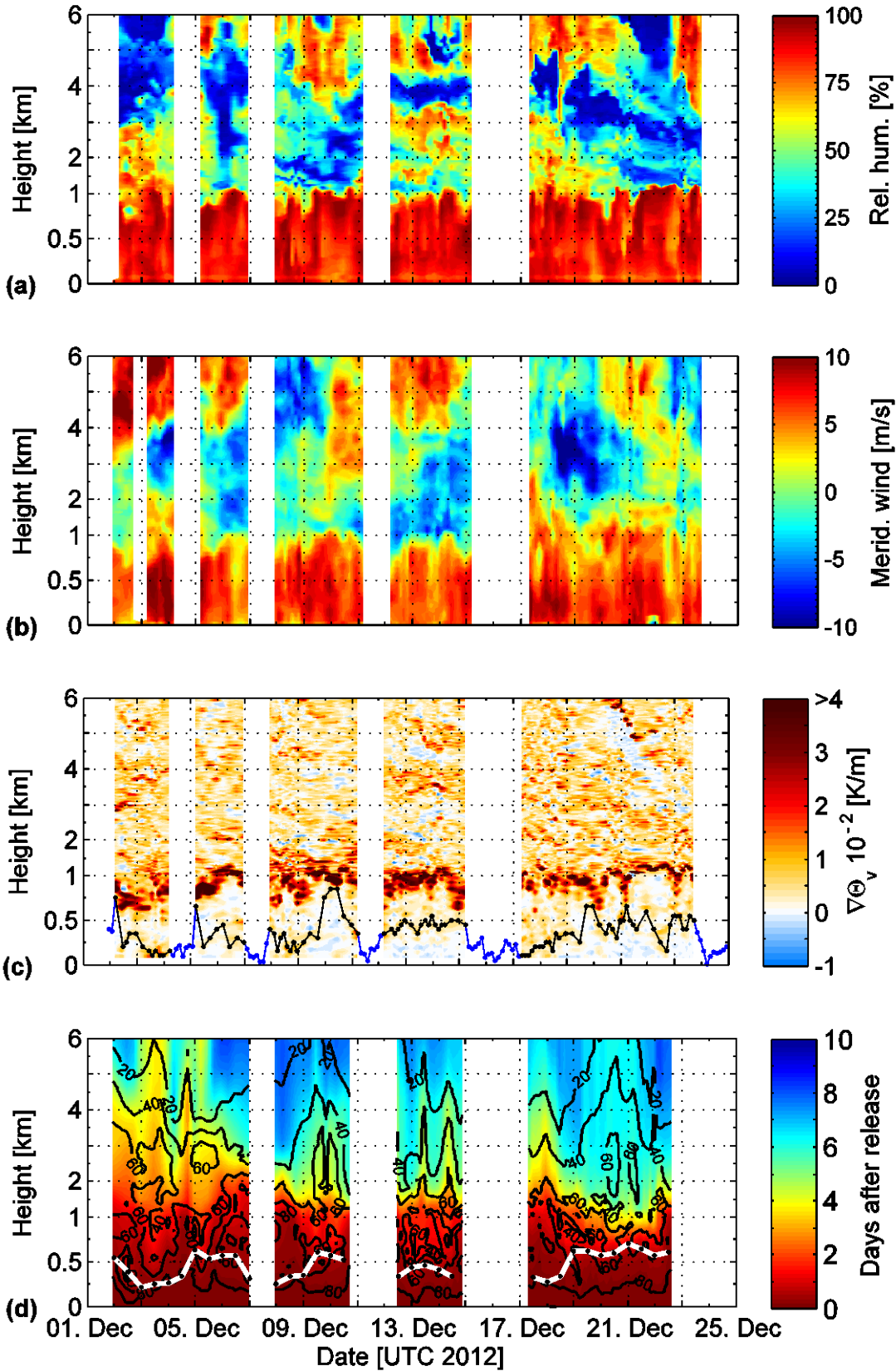


541 Figure 3a-e: Observations during December 1 – 25, 2012 on R/V METEOR. Diurnal stations  
542 are indicated by grey background shades. (a) 10 minute mean of the SAT (orange) and the  
543 SST (blue) in °C. According to SST decrease, upwelling regions are marked with a light blue  
544 background shade in Figure 3b-e. (b) 10 minute mean of wind direction in cardinal directions  
545 (ocher) and wind speed in m/s (blue). (c) 10 minute mean of relative humidity in % (dark  
546 blue) and absolute humidity in  $\text{gm}^{-3}$  (green). (d) Oceanic surface concentrations of  
547 bromoform ( $\text{CHBr}_3$ , blue), dibromomethane ( $\text{CH}_2\text{Br}_2$ , dark grey) and methyl iodide ( $\text{CH}_3\text{I}$ ,  
548 red) in  $\text{pmol L}^{-1}$ . (e) Atmospheric mixing ratios of bromoform, dibromomethane and methyl  
549 iodide in ppt. (f) Concentration ratio of dibromomethane and bromoform. (g) Sea-air flux for  
550 bromoform, dibromomethane and methyl iodide in  $\text{nmol m}^{-2} \text{h}^{-1}$ .

551 Table 1: Oceanic concentrations, atmospheric mixing ratios and sea-air fluxes of bromoform  
 552 ( $\text{CHBr}_3$ ), dibromomethane ( $\text{CH}_2\text{Br}_2$ ), the concentration ratio of bromoform and  
 553 dibromomethane and methyl iodide ( $\text{CH}_3\text{I}$ ) observed during the cruise. Values are given in  
 554 mean  $\pm 1\sigma$ . The range is given in [].

	$\text{CHBr}_3$	$\text{CH}_2\text{Br}_2$	$\text{CH}_2\text{Br}_2 / \text{CHBr}_3$	$\text{CH}_3\text{I}$
Oceanic concentration [ $\text{pmol L}^{-1}$ ]	$6.6 \pm 5.5$ [0.2 – 21.5]	$4.3 \pm 3.4$ [0.2 – 12.7]	$0.9 \pm 0.8$ [0.1 – 4.2]	$9.8 \pm 6.3$ [1.1 – 35.4]
Atmospheric mixing ratio [ppt]	$2.9 \pm 0.7$ [1.5 – 5.9]	$1.3 \pm 0.3$ [0.8 – 2.0]	$0.4 \pm 0.1$ [0.3 – 0.7]	$1.5 \pm 0.5$ [0.6 – 3.2]
Sea-air flux [ $\text{pmol m}^{-2} \text{h}^{-1}$ ]	$117 \pm 492$ [-477 – 1916]	$245 \pm 299$ [-112 – 1169]	$0.4 \pm 8.6$ [-24.5 – 48.9]	$856 \pm 623$ [18 - 4179]

555



556

557

558

559

560

561

562

Figure 4: (a-c) Radiosonde observations of the lower 6 km of the atmosphere between December 2 and 24, 2012 on R/V Meteor. Shown are (a) the relative humidity in %, (b) the meridional wind in m/s and (c) the gradient of the virtual potential temperature in  $10^{-2}$  K/m in

563 combination with the determined MABL height (black) and the complimented MABL height  
564 above the oceanic upwelling from the multiple linear regressions (blue). (d) Distribution of  
565 10-day FLEXPART forward trajectories. The black contour lines give the amount of  
566 trajectories in percentage reaching an altitude of 0 – 6 km height within the 10 days. The  
567 elapsed time in days until these trajectories reach this height is reflected by the colour  
568 shading. The white line shows the ERA-Interim MABL height at the ship position. Trajectory  
569 analyses gaps close to the coast are whitened (Section- 2.4~~2.5~~). The y-axes are non-linear.

570 Table 2: VSLS source-loss calculations: Mean  $\pm 1\sigma$  of Oceanic Delivery (OD), Advective  
 571 Delivery (AD), Chemical Loss (CL), Convective Loss (COL), Oceanic Delivery Ratio  
 572 (ODR), Advective Delivery Ratio (ADR) and Chemical Loss Ratio (CLR) of bromoform  
 573 ( $\text{CHBr}_3$ ), dibromomethane ( $\text{CH}_2\text{Br}_2$ ) and methyl iodide ( $\text{CH}_3\text{I}$ ). Parameters have been  
 574 computed for a box with the vertical extension of the in-situ MABL height (MABLH) and a  
 575 mean trade inversion height (TIH) of 1.1 km.

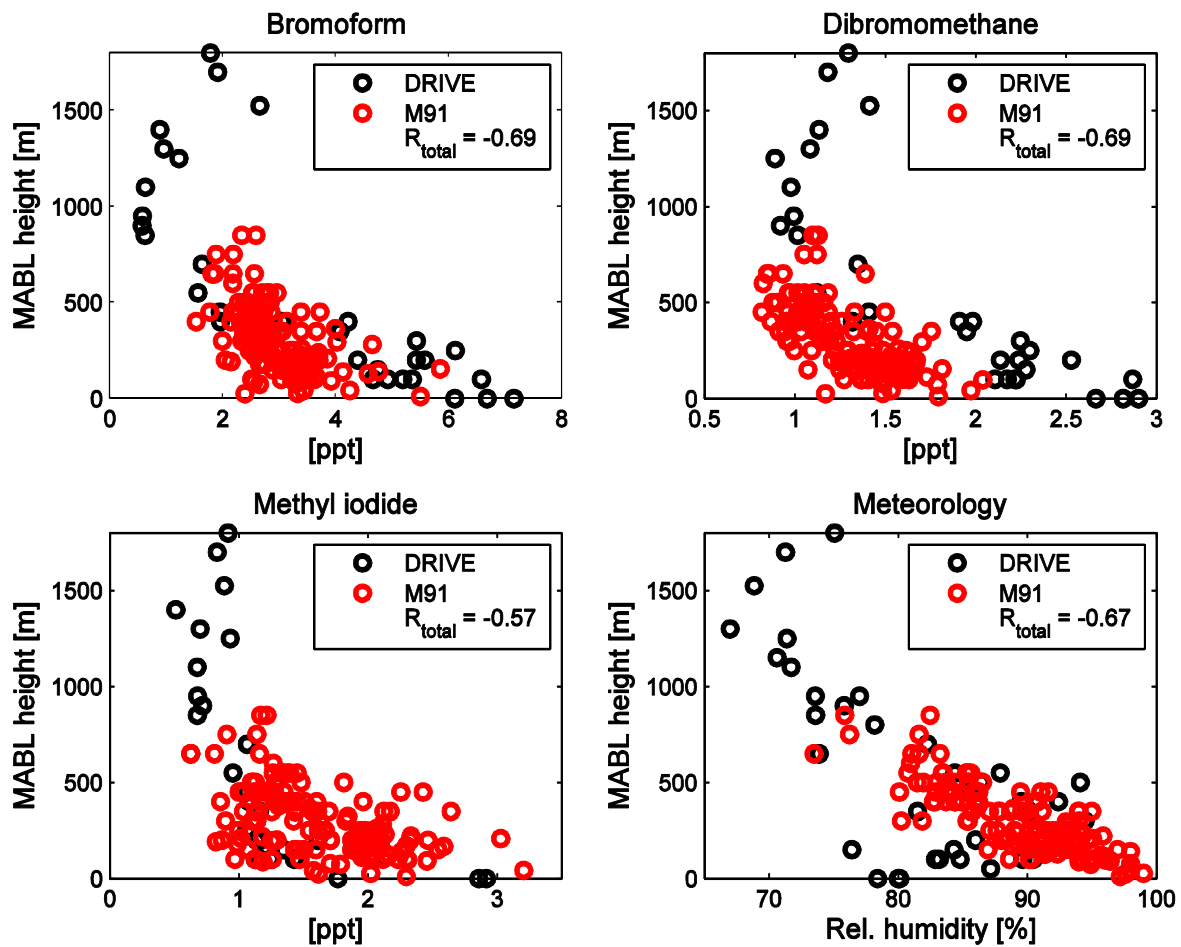
		OD [% d <sup>-1</sup> ]	AD [% d <sup>-1</sup> ]	CL [% d <sup>-1</sup> ]	COL [% d <sup>-1</sup> ]	ODR	ADR	CLR
$\text{CHBr}_3$	MABLH	9.1 $\pm 28.0$	349.0 $\pm 113.4$	7.1	351.0 $\pm 109.4$	0.03 $\pm 0.08$	0.99 $\pm 0.08$	0.02 $\pm 0.01$
	TIH	3.9 $\pm 12.0$	53.2 $\pm 23.2$	7.1	50.0 $\pm 18.4$	0.11 $\pm 0.4$	1.06 $\pm 0.39$	0.17 $\pm 0.07$
$\text{CH}_2\text{Br}_2$	MABLH	32.1 $\pm 38.7$	320.1 $\pm 115.6$	1.2	351.0 $\pm 109.4$	0.10 $\pm 0.11$	0.90 $\pm 0.11$	0.00 $\pm 0.00$
	TIH	13.8 $\pm 16.5$	37.4 $\pm 25.9$	1.2	50.0 $\pm 18.4$	0.33 $\pm 0.54$	0.7 $\pm 0.54$	0.03 $\pm 0.01$
$\text{CH}_3\text{I}$	MABLH	88.9 $\pm 48.1$	286.1 $\pm 119.7$	24.0	351.0 $\pm 109.4$	0.28 $\pm 0.17$	0.80 $\pm 0.16$	0.08 $\pm 0.03$
	TIH	36.8 $\pm 20.5$	37.2 $\pm 32.1$	24.0	50.0 $\pm 18.4$	0.92 $\pm 0.69$	0.64 $\pm 0.55$	0.56 $\pm 0.24$

576

577 Table 3: Spearman correlation coefficients (R) of meteorological parameters, MABL height  
 578 and trade inversion height correlated with atmospheric bromoform (CHBr<sub>3</sub>), dibromomethane  
 579 (CH<sub>2</sub>Br<sub>2</sub>) and methyl iodide (CH<sub>3</sub>I). MABL height\* is the determined MABL height from the  
 580 radiosonde launches, complimented by the regressed MABL height (Section 3.3). Bold  
 581 coefficients are significant with a p-value of < 0.05.

	MABL height	MABL height*	Trade inversion	CHBr <sub>3</sub>	CH <sub>2</sub> Br <sub>2</sub>	CH <sub>3</sub> I
Wind speed	<b>0.35</b>	<b>0.44</b>	-0.06	<b>-0.38</b>	<b>-0.53</b>	<b>-0.33</b>
SAT	<b>0.65</b>	<b>0.79</b>	<b>0.24</b>	<b>-0.50</b>	<b>-0.78</b>	<b>-0.37</b>
SST	<b>0.66</b>	<b>0.80</b>	<b>0.23</b>	<b>-0.57</b>	<b>-0.81</b>	<b>-0.42</b>
SAT – SST	<b>-0.39</b>	<b>-0.47</b>	-0.11	<b>0.38</b>	<b>0.48</b>	<b>0.30</b>
Rel. humidity	<b>-0.77</b>	<b>-0.81</b>	-0.06	<b>0.74</b>	<b>0.77</b>	<b>0.67</b>
MABL height*	-	-	0.08	<b>-0.55</b>	<b>-0.61</b>	<b>-0.45</b>
CHBr <sub>3</sub>	<b>-0.55</b>	<b>-0.60</b>	-0.03	-	<b>0.79</b>	<b>0.79</b>
CH <sub>2</sub> Br <sub>2</sub>	<b>-0.61</b>	<b>-0.72</b>	-0.02	<b>0.79</b>	-	<b>0.66</b>
CH <sub>3</sub> I	<b>-0.45</b>	<b>-0.50</b>	<b>0.30</b>	<b>0.79</b>	<b>0.66</b>	-

582



583

584 Figure 5: Scatter plots of near surface atmospheric mixing ratios of bromoform,  
 585 dibromomethane, methyl iodide and relative humidity vs. MABL height. Black circles reflect  
 586 observations from the DRIVE campaign covering the Mauritanian Upwelling (Fuhlbrügge et  
 587 al., 2013) and red circles from this study (M91) covering the Peruvian Upwelling.  $R_{total}$  gives  
 588 the Spearman correlation coefficients for both data sets together.

589



590 **References**

- 591 Butler, J. H., King, D. B., Lobert, J. M., Montzka, S. A., Yvon-Lewis, S. A., Hall, B. D., Warwick, N. J.,  
592 Mondeel, D. J., Aydin, M., and Elkins, J. W.: Oceanic distributions and emissions of short-lived  
593 halocarbons, *Global Biogeochemical Cycles*, 21, n/a-n/a, 2007.
- 594 Carpenter, L., Fleming, Z., Read, K., Lee, J., Moller, S., Hopkins, J., Purvis, R., Lewis, A., Muller, K.,  
595 Heinold, B., Herrmann, H., Fomba, K., van Pinxteren, D., Muller, C., Tegen, I., Wiedensohler, A.,  
596 Muller, T., Niedermeier, N., Achterberg, E., Patey, M., Kozlova, E., Heimann, M., Heard, D., Plane, J.,  
597 Mahajan, A., Oetjen, H., Ingham, T., Stone, D., Whalley, L., Evans, M., Pilling, M., Leigh, R., Monks, P.,  
598 Karunaharan, A., Vaughan, S., Arnold, S., Tschirter, J., Pohler, D., Friess, U., Holla, R., Mendes, L.,  
599 Lopez, H., Faria, B., Manning, A., and Wallace, D.: Seasonal characteristics of tropical marine  
600 boundary layer air measured at the Cape Verde Atmospheric Observatory, *Journal of Atmospheric*  
601 *Chemistry*, 67, 87-140, 2010.
- 602 Carpenter, L., Liss, P., and Penkett, S.: Marine organohalogens in the atmosphere over the Atlantic  
603 and Southern Oceans, *Journal of Geophysical Research-Atmospheres*, 108, 2003.
- 604 Carpenter, L., Wevill, D., O'Doherty, S., Spain, G., and Simmonds, P.: Atmospheric bromoform at  
605 Mace Head, Ireland: seasonality and evidence for a peatland source, *Atmos. Chem. Phys.*, 5, 2927-  
606 2934, 2005.
- 607 Carpenter, L. J., Reimann, S., Burkholder, J. B., Clerbaux, C., Hall, B. D., Hossaini, R., Laube, J. C., and  
608 Yvon-Lewis, S. A.: Update on Ozone-Depleting Substances (ODSs) and Other Gases of Interest to the  
609 Montreal Protocol. In: *Scientific Assessment of Ozone Depletion: 2014*, Engel, A. and Montzka, S. A.  
610 (Eds.), World Meteorological Organization, Geneva, 2014.
- 611 Codispoti, L. A., Dugdale, R. C., and Minas, H. J.: A comparison of the nutrient regimes off Northwest  
612 Africa, Peru and Baja California, 1982.
- 613 Forster, C., Stohl, A., and Seibert, P.: Parameterization of convective transport in a Lagrangian  
614 particle dispersion model and its evaluation, *Journal of Applied Meteorology and Climatology*, 46,  
615 403-422, 2007.
- 616 Fuhlbrügge, S., Krüger, K., Quack, B., Atlas, E., Hepach, H., and Ziska, F.: Impact of the marine  
617 atmospheric boundary layer conditions on VSLs abundances in the eastern tropical and subtropical  
618 North Atlantic Ocean, *Atmospheric Chemistry and Physics*, 13, 6345-6357, 2013.
- 619 Fuhlbrügge, S., Quack, B., Tegtmeier, S., Atlas, E., Hepach, H., Shi, Q., Raimund, S., and Krüger, K.:  
620 The contribution of oceanic halocarbons to marine and free tropospheric air over the tropical West  
621 Pacific, *Atmos. Chem. Phys.*, 16, 7569-7585, 2016.
- 622 Garreaud, R. and Munoz, R.: The low-level jet off the west coast of subtropical South America:  
623 Structure and variability, *Monthly Weather Review*, 133, 2246-2261, 2005.
- 624 Gómez Martin, J., Mahajan, A., Hay, T., Prados-Roman, C., Ordonez, C., MacDonald, S., Plane, J.,  
625 Sorribas, M., Gil, M., Mora, J., Reyes, M., Oram, D., Leedham, E., and Saiz-Lopez, A.: Iodine chemistry  
626 in the eastern Pacific marine boundary layer, *Journal of Geophysical Research-Atmospheres*, 118,  
627 887-904, 2013.
- 628 Hepach, H., Quack, B., Raimund, S., Fischer, T., Atlas, E., and Bracher, A.: Halocarbon emissions and  
629 sources in the equatorial Atlantic Cold Tongue, *Biogeosciences*, 12, 6369-6387, 2015a.
- 630 Hepach, H., Quack, B., Raimund, S., Fischer, T., Atlas, E. L., and Bracher, A.: Halocarbon emissions  
631 and sources in the equatorial Atlantic Cold Tongue, *Biogeosciences Discuss.*, 12, 5559-5608, 2015b.
- 632 Hepach, H., Quack, B., Tegtmeier, S., Engel, A., Bracher, A., Fuhlbrügge, S., L., G., Atlas, E., Lampel, J.,  
633 Frieß, U., and Krüger, K.: Biogenic halocarbons from the Peruvian upwelling region as tropospheric  
634 halogen source, *Atmos. Chem. Phys. Discuss.*, doi: 10.5194/acp-2016-39, in review, 2016. 2016.
- 635 Hepach, H., Quack, B., Ziska, F., Fuhlbrügge, S., Atlas, E., Krüger, K., Peeken, I., and Wallace, D. W. R.:  
636 Drivers of diel and regional variations of halocarbon emissions from the tropical North East Atlantic,  
637 *Atmos. Chem. Phys.*, 14, 2014.
- 638 Höflich, O.: The meteorological effects of cold upwelling water areas, *Geoforum*, 3, 35-46, 1972.

639 Leedham, E., Hughes, C., Keng, F., Phang, S., Malin, G., and Sturges, W.: Emission of atmospherically  
640 significant halocarbons by naturally occurring and farmed tropical macroalgae, *Biogeosciences*, 10,  
641 3615-3633, 2013.

642 Lennartz, S. T., Krysztofiak, G., Marandino, C. A., Sinnhuber, B. M., Tegtmeier, S., Ziska, F., Hossaini,  
643 R., Krüger, K., Montzka, S. A., Atlas, E., Oram, D. E., Keber, T., Bönisch, H., and Quack, B.: Modelling  
644 marine emissions and atmospheric distributions of halocarbons and dimethyl sulfide: the influence  
645 of prescribed water concentration vs. prescribed emissions, *Atmos. Chem. Phys.*, 15, 11753-11772,  
646 2015.

647 Liu, Y., Yvon-Lewis, S., Thornton, D., Butler, J., Bianchi, T., Campbell, L., Hu, L., and Smith, R.: Spatial  
648 and temporal distributions of bromoform and dibromomethane in the Atlantic Ocean and their  
649 relationship with photosynthetic biomass, *Journal of Geophysical Research-Oceans*, 118, 3950-3965,  
650 2013.

651 Mahajan, A., Martin, J., Hay, T., Royer, S., Yvon-Lewis, S., Liu, Y., Hu, L., Prados-Roman, C., Ordonez,  
652 C., Plane, J., and Saiz-Lopez, A.: Latitudinal distribution of reactive iodine in the Eastern Pacific and its  
653 link to open ocean sources, *Atmospheric Chemistry and Physics*, 12, 11609-11617, 2012.

654 McGivern, W., Sorkhabi, O., Suits, A., Derecskei-Kovacs, A., and North, S.: Primary and secondary  
655 processes in the photodissociation of  $\text{CHBr}_3$ , *Journal of Physical Chemistry a*, 104, 10085-10091,  
656 2000.

657 Nightingale, P., Malin, G., Law, C., Watson, A., Liss, P., Liddicoat, M., Boutin, J., and Upstill-Goddard,  
658 R.: In situ evaluation of air-sea gas exchange parameterizations using novel conservative and volatile  
659 tracers, *Global Biogeochemical Cycles*, 14, 373-387, 2000.

660 O'Brien, L., Harris, N., Robinson, A., Gostlow, B., Warwick, N., Yang, X., and Pyle, J.: Bromocarbons in  
661 the tropical marine boundary layer at the Cape Verde Observatory - measurements and modelling,  
662 *Atmospheric Chemistry and Physics*, 9, 9083-9099, 2009.

663 Quack, B., Atlas, E., Petrick, G., Stroud, V., Schauffler, S., and Wallace, D.: Oceanic bromoform  
664 sources for the tropical atmosphere, *Geophysical Research Letters*, 31, 2004.

665 Quack, B., Atlas, E., Petrick, G., and Wallace, D.: Bromoform and dibromomethane above the  
666 Mauritanian upwelling: Atmospheric distributions and oceanic emissions, *Journal of Geophysical  
667 Research-Atmospheres*, 112, 2007.

668 Quack, B. and Wallace, D. W. R.: Air-sea flux of bromoform: Controls, rates, and implications, *Global  
669 Biogeochemical Cycles*, 17, n/a-n/a, 2003.

670 Raimund, S., Quack, B., Bozec, Y., Vernet, M., Rossi, V., Garcon, V., Morel, Y., and Morin, P.: Sources  
671 of short-lived bromocarbons in the Iberian upwelling system, *Biogeosciences*, 8, 1551-1564, 2011.

672 Rasmussen, R., Khalil, M., Gunawardena, R., and Hoyt, S.: Atmospheric methyl-iodide ( $\text{CH}_3\text{I}$ ), *Journal  
673 of Geophysical Research-Oceans and Atmospheres*, 87, 3086-3090, 1982.

674 Riehl, H.: *Tropical meteorology*. McGraw-Hill, New York-London, 1954.

675 Riehl, H.: *Climate and Weather in the Tropics*, Academic Press, London, 1979.

676 Saiz-Lopez, A., Lamarque, J., Kinnison, D., Tilmes, S., Ordonez, C., Orlando, J., Conley, A., Plane, J.,  
677 Mahajan, A., Santos, G., Atlas, E., Blake, D., Sander, S., Schauffler, S., Thompson, A., and Brasseur, G.:  
678 Estimating the climate significance of halogen-driven ozone loss in the tropical marine troposphere,  
679 *Atmospheric Chemistry and Physics*, 12, 3939-3949, 2012.

680 Saiz-Lopez, A. and von Glasow, R.: Reactive halogen chemistry in the troposphere, *Chemical Society  
681 Reviews*, 41, 6448-6472, 2012.

682 Schauffler, S., Atlas, E., Blake, D., Flocke, F., Lueb, R., Lee-Taylor, J., Stroud, V., and Travnicek, W.:  
683 Distributions of brominated organic compounds in the troposphere and lower stratosphere, *Journal  
684 of Geophysical Research-Atmospheres*, 104, 21513-21535, 1999.

685 Schönhardt, A., Richter, A., Wittrock, F., Kirk, H., Oetjen, H., Roscoe, H., and Burrows, J.:  
686 Observations of iodine monoxide columns from satellite, *Atmospheric Chemistry and Physics*, 8, 637-  
687 653, 2008.

688 Seibert, P., Beyrich, F., Gryning, S., Joffre, S., Rasmussen, A., and Tercier, P.: Review and  
689 intercomparison of operational methods for the determination of the mixing height, *Atmospheric*  
690 *Environment*, 34, 1001-1027, 2000.

691 Simpson, W., Brown, S., Saiz-Lopez, A., Thornton, J., and von Glasow, R.: Tropospheric Halogen  
692 Chemistry: Sources, Cycling, and Impacts, *Chemical Reviews Article ASAP*, doi: 10.1021/cr5006638,  
693 2015. 4035-4062, 2015.

694 Stohl, A., Forster, C., Frank, A., Seibert, P., and Wotawa, G.: Technical note: The Lagrangian particle  
695 dispersion model FLEXPART version 6.2, *Atmospheric Chemistry and Physics*, 5, 2461-2474, 2005.

696 Stohl, A., Hittenberger, M., and Wotawa, G.: Validation of the Lagrangian particle dispersion model  
697 FLEXPART against large-scale tracer experiment data, *Atmospheric Environment*, 32, 4245-4264,  
698 1998.

699 Stohl, A. and Thomson, D.: A density correction for Lagrangian particle dispersion models, *Boundary-*  
700 *Layer Meteorology*, 90, 155-167, 1999.

701 Stohl, A. and Trickl, T.: A textbook example of long-range transport: Simultaneous observation of  
702 ozone maxima of stratospheric and North American origin in the free troposphere over Europe,  
703 *Journal of Geophysical Research-Atmospheres*, 104, 30445-30462, 1999.

704 Stull, R.: *An Introduction to Boundary Layer Meteorology*, Kluwer Academic Publishers, Dordrecht,  
705 1988.

706 Yokouchi, Y., Hasebe, F., Fujiwara, M., Takashima, H., Shiotani, M., Nishi, N., Kanaya, Y., Hashimoto,  
707 S., Fraser, P., Toom-Sauntry, D., Mukai, H., and Nojiri, Y.: Correlations and emission ratios among  
708 bromoform, dibromochloromethane, and dibromomethane in the atmosphere, *Journal of*  
709 *Geophysical Research-Atmospheres*, 110, 2005.

710 Yokouchi, Y., Osada, K., Wada, M., Hasebe, F., Agama, M., Murakami, R., Mukai, H., Nojiri, Y.,  
711 Inuzuka, Y., Toom-Sauntry, D., and Fraser, P.: Global distribution and seasonal concentration change  
712 of methyl iodide in the atmosphere, *Journal of Geophysical Research-Atmospheres*, 113, 2008.

713 Ziska, F., Quack, B., Abrahamsson, K., Archer, S., Atlas, E., Bell, T., Butler, J., Carpenter, L., Jones, C.,  
714 Harris, N., Hepach, H., Heumann, K., Hughes, C., Kuss, J., Kruger, K., Liss, P., Moore, R., Orlikowska,  
715 A., Raimund, S., Reeves, C., Reifenhauer, W., Robinson, A., Schall, C., Tanhua, T., Tegtmeier, S.,  
716 Turner, S., Wang, L., Wallace, D., Williams, J., Yamamoto, H., Yvon-Lewis, S., and Yokouchi, Y.: Global  
717 sea-to-air flux climatology for bromoform, dibromomethane and methyl iodide, *Atmospheric*  
718 *Chemistry and Physics*, 13, 8915-8934, 2013.

719